Geophysical Research Letters

Supporting Information for

Evidence for the maintenance of slowly varying equatorial currents by intraseasonal variability

Richard J. Greatbatch[1,2], Martin Claus[1,2], Peter Brandt[1,2], Jan-Dirk Matthießen[1], Franz Philip Tuchen[1], François Ascani[3], Marcus Dengler[1], John Toole[4], Christina Roth[1] and J. Thomas Farrar[4]

[1]Ocean Circulation and Climate Dynamics, GEOMAR Helmholtz Centre for Ocean Research Kiel, Kiel, Germany
[2]Faculty of Mathematics and Natural Sciences, Christian-Albrechts-Universität zu Kiel, Germany
[3]Department of Oceanography, University of Hawaii, Hawaii, USA
[4]Woods Hole Oceanographic Institution, Woods Hole, MA, USA

Contents of this file:

Text S1, Figures S1, S2, S3, S4 and Table S1.

Introduction

In the Supporting Information we first derive the equations for the convergence of the meridional flux of zonal momentum at the equator. We then give the details of the model set-up and of the analysis applied to the model output, after which we focus on the analysis of the mooring data.

Methods

<u>The meridional flux of intraseasonal zonal momentum</u>

The zonal momentum equation is given by

$$\frac{\partial u}{\partial t}+\frac{\partial(uu)}{\partial x}+\frac{\partial(uv)}{\partial y}+\frac{\partial(uw)}{\partial z}-\beta yv=-\frac{1}{\rho_0}\frac{\partial p}{\partial x}+D \qquad \text{(S1)}$$

where here Cartesian coordinates have been used, for simplicity, with x increasing eastward, y northward and z upward, with corresponding velocity components u, v and w, respectively, p is the pressure and ρ_0 is a representative density for sea water. The equation has been written for an equatorial beta-plane with y = 0 at the equator, and D represents dissipation. In order to focus on the time scales longer than intraseasonal, a temporal low-pass filter, represented by an overbar, is applied (at fixed height) to give

$$\frac{\partial \bar{u}}{\partial t}+\frac{\partial(\bar{u}\bar{u})}{\partial x}+\frac{\partial(\bar{u}\bar{v})}{\partial y}+\frac{\partial(\bar{u}\bar{w})}{\partial z}-\beta y\bar{v}=-\frac{\partial(\overline{u'u'})}{\partial x}-\frac{\partial(\overline{u'v'})}{\partial y}-\frac{\partial(\overline{u'w'})}{\partial z}-\frac{1}{\rho_0}\frac{\partial \bar{p}}{\partial x}+\bar{D} \qquad \text{(S2)}$$

where the local time derivative has been retained to represent the slow time variation of the equatorial currents compared to that of the primed variables which represent the intraseasonal variability. It is implicit in the above that the low-pass filter satisfies the Reynolds condition, i.e. that terms of the form $\overline{\bar{u}v'}$ can be neglected. The vertical momentum flux convergence, $-\frac{\partial(\overline{u'w'})}{\partial z}$, due to internal waves encountering critical layers, has been proposed as a mechanism for accelerating the deep jets [Muench and Kunze, 2000]. However, since our model does not adequately resolve internal waves but still realistically reproduces the jets, this term is not discussed further here. The dominant balance in (S2) at the equator (y = 0) is then given by

$$\frac{\partial \bar{u}}{\partial t}\approx-\frac{\partial(\overline{u'v'})}{\partial y}-\frac{1}{\rho_0}\frac{\partial \bar{p}}{\partial x}+dissipation \quad , \qquad \text{(S3)}$$

where, here, the dissipation includes not only the low-pass filter of D but also contributions from the other terms in the averaged equation (e.g. the zonal advection terms) that are associated with dissipation [*Ascani et al.*, 2015]. The meridional flux of intraseasonal zonal momentum is given by $\overline{u'v'}$ and its convergence at the equator by $-\frac{\partial(\overline{u'v'})}{\partial y}$.

Model Set-up

The model simulations were carried out using the MITgcm [*Marshall et al.*, 1997] with a horizontal grid resolution of 0.25° and 200 levels in the vertical with a finer resolution in the upper part of the water column than further down [*Ascani et al.*, 2015; *Matthießen et al*., 2015, 2017]. The model domain is a rectangular basin in latitude/longitude space with a flat bottom at depth 5000 m, closed walls at the northern, southern, western, and eastern boundaries, a width of 72^{o} in the zonal direction and extends meridionally from 20°S to 20°N. Vertical mixing is parameterized using a Richardson number dependent scheme [*Pacanowski and Philander*, 1981] with a background vertical diffusivity of 10^{-5} m^2 s^{-1} and biharmonic friction is used in the horizontal for both tracers and momentum with coefficient 2 x 10^{10} m^4 s^{-1}. The bottom friction is set to zero and the model is forced at the surface by a time-independent wind stress that is switched on at the start of the integration, the model being initialized in a state of rest with a specified horizontally uniform density stratification. The wind stress is zonally uniform and is the zonal average of the annual mean wind stress from NCEP [*Kalnay et al.*, 1996]. Potential temperature is the only active tracer, salinity being kept constant and uniform at 35 psu, and a linear equation of state is used, as in *Ascani et al.* [2015] and *Matthießen et al*.[2015, 2017]. The initial potential temperature field is obtained by area-averaging potential temperature at each depth from the World Ocean Atlas [*Levitus et al*., 2013] within the region of the Atlantic Ocean corresponding to the latitude range of the model domain. Throughout the integrations, the surface temperature is relaxed to the initial surface temperature with a time scale of 30 days.

Vertical mode decomposition from model output

The mean potential temperature profile T(z), diagnosed over the whole 180 years of model integration at the center of the basin and averaged between 2.5°S and 2.5°N, was used to compute a mean buoyancy frequency profile from the linear equation of state used by the model. Based on this profile the baroclinic vertical structure functions are computed by numerically solving the eigenvalue problem of Sturm-Liouville type [*Gill*, 1982]

$$\frac{d}{dz}\left[\frac{1}{N^2}\frac{d\hat{p}_n}{dz}\right]+\frac{1}{c_n^2}\hat{p}_n=0$$

with boundary conditions $\frac{1}{N^2}\frac{d\hat{p}_n}{dz}=0$ at the bottom and $\hat{p}_n+\frac{g}{N^2}\frac{d\hat{p}_n}{dz}=0$ at the surface. g is the acceleration due to gravity. The result is an orthogonal set of vertical structure functions, $\hat{p}_n$ and associated constants c_n representing the phase speed of gravity waves for a particular vertical mode. The vertical mode amplitudes are normalized such that

$$\int_{-H}^{0} \hat{p}_n^2 dz = H ,$$

where *H* is the depth of the model ocean (here 5000 m). The horizontal velocity components can now be expanded in terms of vertical modes as

$$(u,v) = \sum_{n=0}^{\infty} (u_n, v_n) \hat{p}_n ,$$

where u_n and v_n are the projection of *u* and *v*, respectively, onto the nth vertical mode given by

$$(u_n, v_n) = \frac{1}{H} \int_{-H}^{0} (u,v) \hat{p}_n dz .$$

<u>The flux of intraseasonal zonal momentum from model output</u>

The model was used to produce 180 years of 5-daily instantaneous output of which the first 75 years were considered as model spin up and were discarded for the analysis. The horizontal velocity components were separated into a low frequency and a high frequency part by using a temporal low-pass filter having a cut-off period of 70 days and the filter is a weighted moving average using a Hanning window as weights. It should be noted that this form of low-pass filter is not guaranteed to exactly satisfy the Reynolds condition that has been used to derive equations (S2) and (S3). However, given the spectral gap between the time scale of the deep jets (several years) and that of the intraseasonal variability, the error should be small. Unlike the mooring data (see below), we do not apply a 20 day low-pass filter before applying the 70 day low-pass filter since we do not have tides, and only weak internal waves, in the model. To be comparable to the results from the observations the convergence of the meridional flux of intraseasonal zonal momentum in the center of the basin is computed as the difference in the flux between 0.75°S and 0.75°N divided by the distance between the two locations. For Figure 4a, the time mean of the convergence of the flux of intraseasonal zonal momentum was first removed followed by the application of an additional 70 day low-pass filter before plotting.

For the regression of the convergence of the momentum flux on the slowly varying equatorial zonal velocity shown in Figure 5, the additional 70 day low-pass filter was not applied. This was done in order to ensure comparability with the regression based on the mooring data for which the convergence of the momentum flux was not low-pass filtered. To account for the autocorrelation of the time series of both the intraseasonal zonal and meridional velocity fluctuations, the estimate of the standard error of the regression slope is scaled by $\sqrt{(1+r_x r_y)/(1-r_x r_y)}$ where r_x and r_y are the autocorrelation coefficients of each time series at lag 1 (here 5 days), following *Bretherton et al.*[1999].

<u>Modal decomposition of the power input</u>

The power input by the convergence of the meridional flux of intraseasonal zonal momentum into the slowly varying equatorial zonal velocity is given by

$$P = -\rho_0 \bar{u} \frac{\partial}{\partial y} \overline{u'v'} .$$

The vertical integral of the power input can be expressed by expanding the intraseasonal velocity fluctuations into vertical modes as

$$\int_{-H}^{0} P dz = -\rho_0 \int_{-H}^{0} \bar{u} \frac{\partial}{\partial y} \overline{\sum_{n=0}^{\infty} \hat{p}_n u'_n \sum_{m=0}^{\infty} \hat{p}_m v'_m} dz = -\rho_0 \sum_{n=0}^{\infty} \sum_{m=0}^{\infty} \frac{\partial}{\partial y} \overline{u'_n v'_m} \int \bar{u} \hat{p}_n \hat{p}_m dz .$$

This allows us to diagnose the contribution of the intraseasonal fluctuations associated with different vertical modes to the vertically-integrated power input. This is done by evaluating the above expression for individual pairs (n, m), where n and m are the vertical mode numbers of the intraseasonal zonal and meridional velocity fluctuations, respectively, to give:

$$P_{nm} = -\rho_0 \frac{\partial}{\partial y} \overline{u'_n v'_m} \int_{-H}^{0} \bar{u} \hat{p}_n \hat{p}_m dz .$$

<u>Mooring Data</u>

For this study, we used horizontal velocity data obtained from an equatorial current meter mooring at 23°W deployed from 2002 to 2016. The dataset is an update of that described in *Bunge et al.*[2008], *Brandt et al.* [2016] and *Claus et al.* [2016]. From 2006 to 2011, the equatorial mooring was part of a moored array along 23°W installed for three mooring periods. The mooring array consisted of three moorings located at 0.75°S, the equator, and 0.75°N, and was first deployed in June 2006, serviced in February 2008 and October 2009, and finally recovered in June 2011. The equatorial mooring was equipped with two acoustic Doppler current profilers (ADCPs): one 150 kHz upward looking instrument at a depth of about 200 m and another 75 kHz instrument either downward looking from just below the upper instrument or upward looking from larger depth. Unfortunately, the upper instrument failed during the first mooring period June 2006 to February 2008 leading to a slightly reduced measurement range. At the off-equatorial moorings, we used only upward looking instruments, either 150 kHz or 75 kHz leading to slightly varying depth ranges. All velocities were detided using a 40 hour low-pass filter and subsampled to 12 hour intervals. Here, we used only velocity data from two depth ranges, i.e. 56 to 150m and 300 to 500m. Additionally, we used horizontal velocity data from two McLane Moored Profilers (MMP) installed at the moorings at 0.75°S and at the equator during the mooring period from October 2009 to June 2011. They covered the common depth range 1090 to 3490 m. The MMPs were programmed to occupy profiles in bursts of two one-way traverses every 4 days, with the one-way profiles initiated 6 h apart. No temporal filter was applied to the acquired velocity data. The oceanic variability on intraseasonal timescales clearly exceeds the measurement accuracy of the different instruments in use.

Vertical mode decomposition from observations

Shipboard CTD measurements taken during the mooring service cruises were used to calculate individual buoyancy frequency profiles that were averaged to derive a mean buoyancy frequency profile N^2 for the depth range 0 to 4500 m. The subsequent computation of the baroclinic vertical structure functions and their normalization were performed identical to the model analysis with the depth, H, set to the maximum depth of the buoyancy frequency profile (here 4500 m).

The flux of intraseasonal zonal momentum from observations

Zonal and meridional velocity data were taken from three different moorings (each consisting of three mooring periods between 2006-2011) along 23°W at 0.75°S, equator, and 0.75°N. All data were low-pass filtered with a cut-off period of 20 days to reduce short timescale noise. For the Reynolds-averaging, the resulting velocities were separated into slowly varying (marked by an overbar) and fluctuating (marked by a prime) components:

$$u = \bar{u} + u', v = \bar{v} + v'.$$

The slowly varying components were derived by applying a 70-day low-pass filter particularly removing the intraseasonal variability having a dominant period of about 30 days (Figure S3A shows the equatorial zonal velocity as an example). The fluctuating components were then derived by subtracting the slowly varying components from the 20 day low-pass filtered time series. The convergence of the meridional flux of intraseasonal zonal momentum was calculated using the fluctuating components from pairs of moorings: 1) North-South uses data from moorings at 0.75°N and 0.75°S (Figure S3B), 2) North-Equator uses data from moorings at 0.75°N and the equator (Figure S3C) and 3) Equator-South uses data from moorings at the equator and 0.75°S (Figure S3D). It should be noted that below 1000 m, only the moorings at and south of the equator are available and this only for roughly 18 months in 2010 and 2011 (Figure S3D).

For the depth range 300 to 500 m, the slowly varying zonal velocity at the equator was further separated into seasonal and interannual components. The interannual component was derived by subtracting the semi-annual and annual harmonics from the slowly varying zonal velocity followed by the application of a 270 day low-pass filter. The seasonal component was then derived by subtracting the interannual component from the slowly varying component (Figure S4). For each filter application the lengths of the time-series were reduced by half the window size at the beginning and at the end of the time series.

In a next step, the regression of the convergence of the meridional flux of intraseasonal zonal momentum on the slowly varying equatorial zonal velocity was calculated. Before calculating the regression the time-averaged zonal velocity was subtracted from the slowly varying zonal velocity. This was done only in the upper 500 m as below the mean was generally weak and not well-enough determined from the available data. To estimate the standard error of the regression slopes, the degrees of freedom (DoF) for the following data blocks were obtained: 1) the Equatorial Undercurrent range from 56 to 150 m, 2) the shallow Equatorial Deep Jet (EDJ) range from 300 to 500m, 3) the deep EDJ range from 1090 to 2000 m, and 4) the deepest EDJ range 2000 to 3490 m. The choice of 2000 m is based on noting that when computing the regression slope at each depth separately, a clear regime change occurs near 2000 m depth, with the sign of the slope changing as shown in Figure 5. The DoF were calculated from the autocorrelations of the time series and profiles, respectively, of the slowly varying equatorial zonal velocity and the convergence of the meridional flux of intraseasonal zonal momentum from each data block. The decorrelation time and space scales were estimated as the lags at which the autocorrelation functions averaged over all depth levels and time steps, respectively, fall below e^{-1}. Here, always the largest time and space scales of the two quantities to be regressed on each other were chosen. The total DoF for each block were then calculated by multiplying the length of the time series and the length of the depth vector divided by their respective decorrelation time and space scales. The resulting regression slopes between the slowly varying zonal velocity at the equator and the convergence of the meridional flux of intraseasonal zonal momentum are given in Table S1 together with its standard error and the DoF for different depth ranges and mooring pairs. Also given are the statistical quantities when the slowly varying zonal velocity is separated into an interannual and a seasonal component.

Finally, we note that the low-pass filters applied to the mooring data are not guaranteed to exactly satisfy the Reynolds condition that is assumed in deriving equations (S2) and (S3) above. As for the model data, this is unlikely to pose a problem for our explanation for the maintenance of the deep jets given the large spectral gap between the time scale of the deep jets (4.5 years) and that of the intraseasonal variability. However, the resulting error could be larger in the case of the annual and semi-annual period variability, especially the latter for which a clear spectral gap is not present.

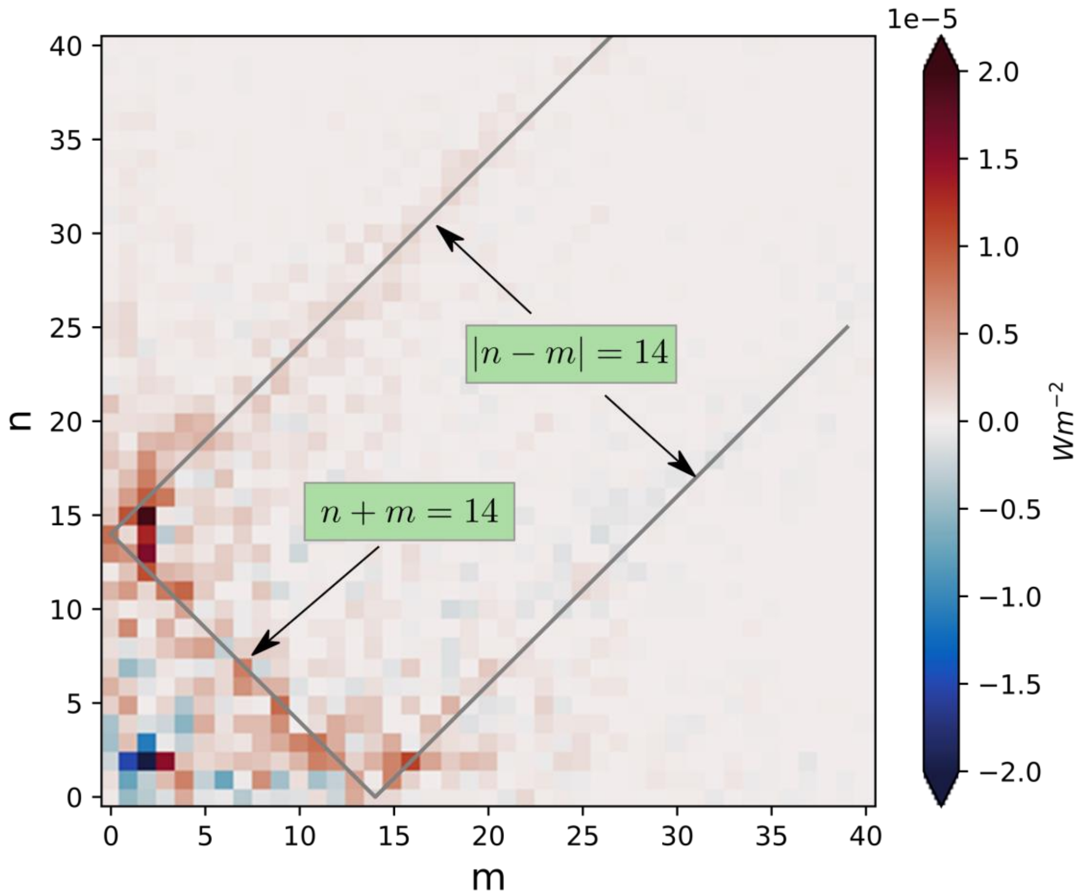

Figure S1. Power input associated with the different vertical normal modes, P_{nm}, to the slowly varying zonal velocity at the equator in the model. Note that the power input originates, to a good approximation, from pairs of vertical mode numbers that add up to or differ by 14, the dominant vertical mode associated with the deep jets in the model. The details of the computation of P_{nm} can be found in the Supporting Information, above. Note also that the P_{nm} shown have been time-averaged over the full analysis period of 105 years.

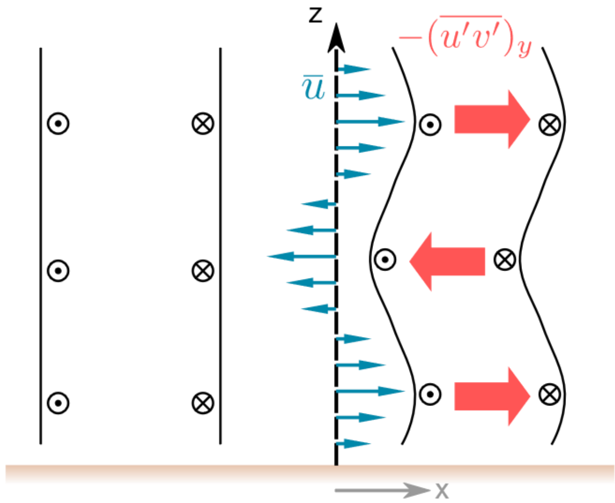

Figure S2. The distortion of intraseasonal waves by the deep jets shown schematically for the vertical plane. An initially barotropic wave (left hand panel) is advected by the deep jets (shown by the blue arrows) in such a way as to generate an intraseasonal wave with the same vertical structure as the deep jets (right hand panel). The corresponding momentum flux convergence is shown in red. $\odot$/$\otimes$ indicates southward/northward flow associated with the intraseasonal wave.

(A)

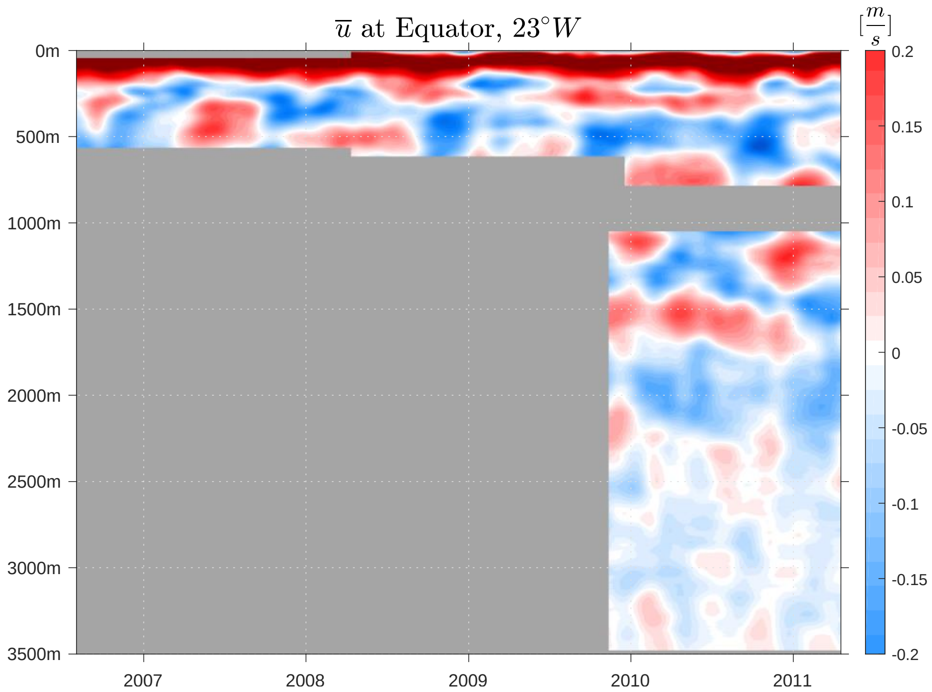

$\overline{u}$ at Equator, 23°W
$[\frac{m}{s}]$
0m
500m
1000m
1500m
2000m
2500m
3000m
3500m
2007
2008
2009
2010
2011
0.2
0.15
0.1
0.05
0
-0.05
-0.1
-0.15
-0.2

(B)

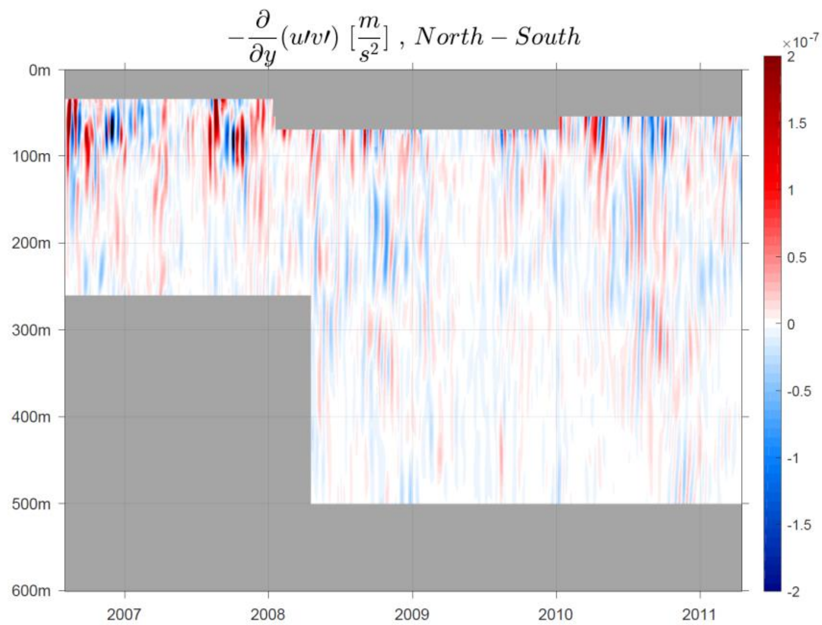

$-\frac{\partial}{\partial y}(u\prime v\prime)\ [\frac{m}{s^2}]\ ,\ North - South$
×10^-7
0m
100m
200m
300m
400m
500m
600m
2007
2008
2009
2010
2011
2
1.5
1
0.5
0
-0.5
-1
-1.5
-2

(C)

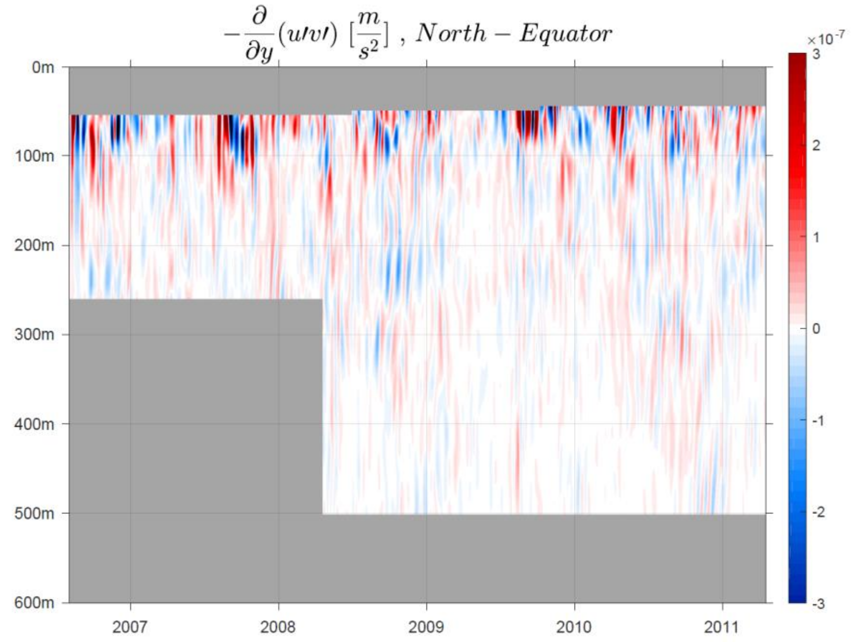
$-\frac{\partial}{\partial y}(u'v')\ [\frac{m}{s^2}]$, $North - Equator$
0m
100m
200m
300m
400m
500m
600m
2007
2008
2009
2010
2011
$\times 10^{-7}$
3
2
1
0
-1
-2
-3

(D)

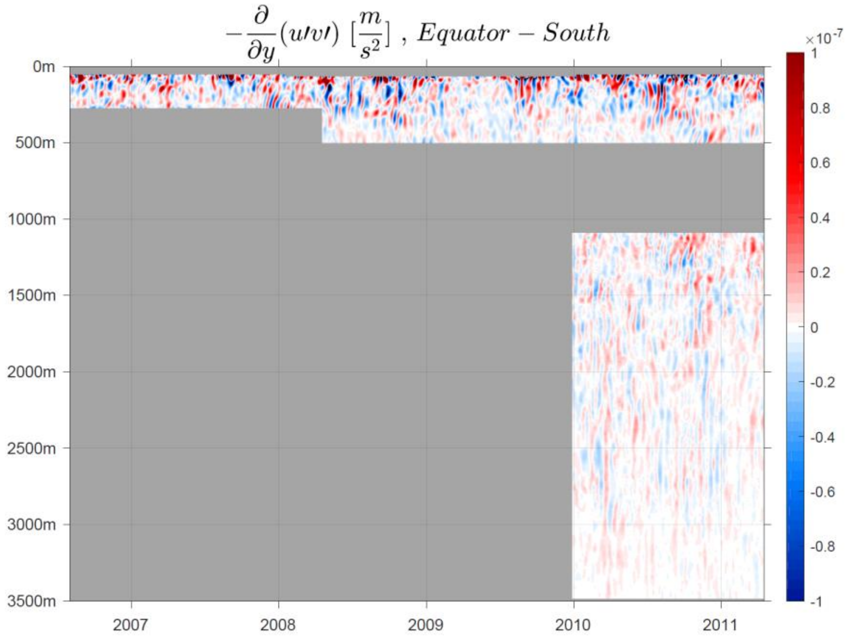
$-\frac{\partial}{\partial y}(u'v')\ [\frac{m}{s^2}]$, $Equator - South$
0m
500m
1000m
1500m
2000m
2500m
3000m
3500m
2007
2008
2009
2010
2011
$\times 10^{-7}$
1
0.8
0.6
0.4
0.2
0
-0.2
-0.4
-0.6
-0.8
-1

Figure S3. Available time series of velocity data and derived quantities as a function of depth [m] and time [yr] from the equatorial mooring array along 23°W. The slowly varying zonal velocity [m s^{-1}] (A) was derived from the equatorial mooring. The convergence of the meridional flux of intraseasonal zonal momentum [10^{-7} m s^{-2}] was derived from the mooring pairs (B) at 0.75°N and 0.75°S, (C) at 0.75°N and at the equator and (D) at the equator and 0.75°S.

(A)

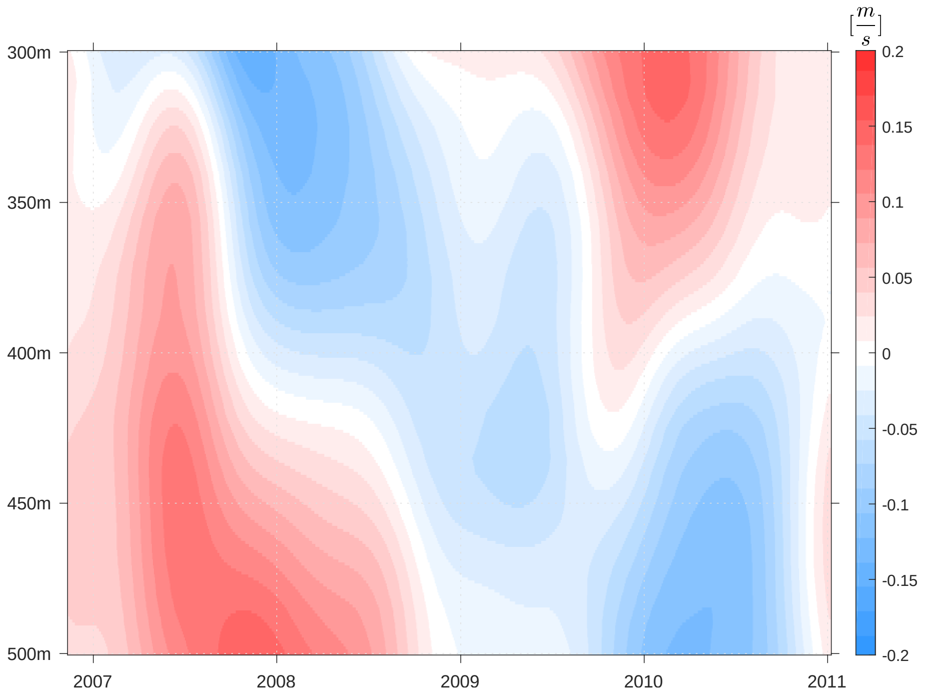

(B)

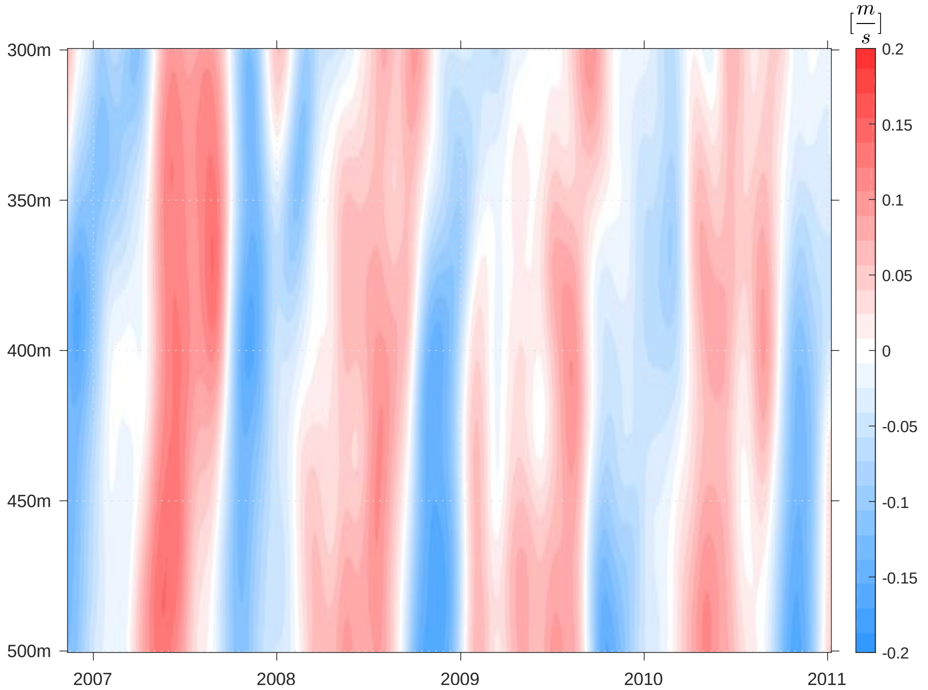

Figure S4. Slowly varying zonal velocity at the equator as a function of depth [m] and time [yr] from the equatorial mooring at 23°W, separated into an interannual component (A) and a seasonal component (B). See the section on "The flux of intraseasonal zonal momentum from observations" in the Supporting Information, above, for the details of the derivation of the two components.

Table S1. Statistics of the regression analysis from the mooring data. Given is the slope of the regression, b in [s^{-1}], its standard error, σ in [s^{-1}], and the number of degrees of freedom, N.

Depth \ Moorings	**0.75°N – 0.75°S**	**0.75°N –Equator**	**Equator –0.75°S**
56-150m		b = -1.77e-8 σ = 1.60e-8 N = 224	
70-150m	b = -1.53e-8 σ = 6.69e-9 N = 186		b = -2.17e-8 σ = 1.23e-8 N = 186
300-500m	b = 1.02e-8 σ = 3.85e-9 N = 85	b = 1.38e-8 σ = 6.39e-9 N = 85	b = 6.62e-9 σ = 4.72e-9 N = 85
1090-2000m			b = 5.68e-9 σ = 4.23e-9 N = 81
2000-3490m			b = -3.95e-9 σ = 3.92e-9 N = 182

Separation into interannual and seasonal components

300-500m (interannual component)	b = 1.07e-8 σ = 4.23e-9 N = 40	b = 7.87e-9 σ = 8.03e-9 N = 40	b = 1.35e-8 σ = 6.58e-9 N = 40
300-500m (seasonal component)	b = 7.24e-9 σ = 3.75e-9 N = 114	b = 6.40e-9 σ = 6.42e-9 N = 114	b = 8.09e-9 σ = 6.25e-9 N = 114

References:

Ascani, F., Firing, E., McCreary, J.P., Brandt, P., & Greatbatch, R.J. (2015). The deep equatorial ocean circulation in wind-forced numerical solutions. *J. Phys. Oceanogr.*, 45, 1709-1734.

Brandt, P., Claus, M., Greatbatch, R.J., Kopte, R., Toole, J.M., Johns, W.M. & Böning, C.W. (2016). Annual and semiannual cycle of equatorial Atlantic circulation associated with basin mode resonance. *J. Phys. Oceanogr.*, 46, 3011-3029.

Bretherton, C. S., Widmann, M., Dymnikov, V. P., Wallace, J. M. & Blad, I. (1999). The effective number of spatial degrees of freedom of a time-varying field. *J. Clim.*,12,1990-2009. doi:10.1175/15200442(1999)012<1990:TENOSD>2.0.CO;2.

Bunge, L., Provost, C., Hua, B. L. & Kartavtseff, A. (2008). Variability at intermediate depths at the equator in the Atlantic Ocean in 2000–06: annual cycle, equatorial deep jets, and intraseasonal meridional velocity fluctuations. *J. Phys. Oceanogr.*, 38, 1794–1806. doi: 10.1175/2008JPO3781.1.

Claus, M., Greatbatch, R.J., Brandt, P. & Toole, J.M. (2016). Forcing of the Atlantic equatorial deep jets derived from observations. *J. Phys. Oceanogr.*, 46, 3549-3562.

Gill, A. E. (1982), Atmosphere–Ocean Dynamics. Academic Press, 664 pp..

Kalnay, E., Kanamitsu, M., Kistler, R., Collins, W., Deaven, D., Gandin, L., ... & Zhu, Y. (1996). The NCEP/NCAR 40-year reanalysis project. *Bulletin of the American Meteorological Society*, 77, 437-471.

Levitus, S., Antonov, J.I., Baranova, O.K., Boyer, T.P., Coleman, C.L., Garcia, H.E., Grodsky, A.I., Johnson, D.R., Locarnini, R.A., Mishonov, A.V. and Reagan, J.R. (2013). The world ocean database. *Data Science Journal*, 12, WDS229-WDS234.

Marshall, J., Adcroft, A., Hill, C., Perelman, L., & Heisey, C. (1997). A finite-volume, incompressible Navier Stokes model for studies of the ocean on parallel computers. *J. Geophys. Res.*, 102, 5753-5766.

Matthießen, J.-D., Greatbatch, R.J., Brandt, P., Claus, M. & Didwischus, S.-H. (2015). Influence of the equatorial deep jets on the North Equatorial Countercurrent. *Ocean Dynamics*, 65, 1095-1102.

Matthießen, J.-D., Greatbatch, R.J., Claus, M., Ascani F. and Brandt, P. (2017). The emergence of equatorial deep jets in an idealised primitive equation model: an interpretation in terms of basin modes. *Ocean Dynamics*, 67, 1511-1522.

Muench, J.E., and Kunze, E. (2000). Internal wave interactions with equatorial deep jets. Part II: Acceleration of the jets. *J. Phys. Oceanogr.*, 30, 2099-2110.

Pacanowski, R. C., & Philander, S. G. H (1981). Parameterization of vertical mixing in numerical models of tropical oceans. *J. Phys. Oceanogr.,* 11, 1443-1451.